Please do not adjust margins

Journal Name

COMMUNICATION

Duplex nanoporous alumina and polyelectrolyte adsorption: more insights from a combined neutron reflectivity and electron microscopy study

Received 00th January 20xx,
Accepted 00th January 20xx

DOI: 10.1039/x0xx00000x

www.rsc.org/

Anastasia Christoulaki,[a] Alexis Chennevière, [b] Emmanuelle Dubois, [a] and Nicolas Jouault*[a]

Neutron reflectivity (NR) is a powerful technique to investigate the incorporation of nanomaterials (polymers, nanoparticles,…) into multilayers porous systems. Here we propose an experimental approach combining NR and scanning electron microscopy (SEM) to successfully characterize duplex nanoporous anodic aluminum oxide (nAAO) and to extract quantitative information about the entering and adsorption of polyelectrolytes (PE) in nanopores. Duplex nAAO are promising systems to study the influence of geometrical constriction, i.e. reduction of pore diameter along the pore channel, on the confinement of condensed matter.

Nanoporous anodic alumina oxides (nAAO) are very promising host systems for confinement studies. nAAO are obtained through the controlled anodization of aluminum (Al) in acidic electrolytes and are composed of high-ratio parallel cylindrical channels with perfectly tunable pore diameters, interpore distances, lengths and porosity. Several studies have explored the potential applications of nAAO such as biosensors[1], templates for the growth of functional materials[2], ion selective membranes[3], filtration or chemical separation devices, making nAAO interesting materials for many purposes.

Since the pioneering work of Masuda and Fukuda in 1995 who proposed a two-step anodization process to produce very ordered nanopores[4], new experimental strategies have been developed to synthesize more complex nAAO with variable and modulated morphologies using anodization/chemical etching sequences[5], current pulses[6] or cyclic current gradients[7]. Among these new structures, bilayers or "duplex" nAAO are composed of two connected layers having similar pore density but different pore diameters D_p[8]: one top layer with large D_p followed by a bottom layer with smaller D_p (see scheme in Fig. 1c). Such organization induces a geometrical constriction, i.e. a reduction of pore diameter along the pore channel, that plays an important role for instance in gas adsorption and condensation[9-11].

Duplex nAAO systems require original and suitable experimental strategies to characterize at the nanometer scale the different layers and also to investigate the behavior of incorporated nano-objects such as liquid crystals[12], liquid mixtures[13], polymer melts[14] or polyelectrolytes[15] (PEs). In particular the latter case of PE confinement is barely studied while it is of great interest for nanofluidic or biological applications as sequencing of DNA strands, designing pores for biosensors and selectivity properties[16], filtration or chemical separation or for more fundamental aspects such as the understanding of protein insertion[17] and translocation into biological membranes.

So far, duplex structures have been scarcely studied and were primarily characterized by direct imaging (Scanning Electron Microscopy)[9, 10] and interferometry techniques using light radiation[9, 15]. Here we demonstrate that specular Neutron Reflectivity (NR) is a powerful technique to extract quantitative information about the structure and composition of duplex nAAO and also provides information about the PE behavior in nanopores at the molecular level. Because of the use of short wavelengths and the fact that neutrons are strongly scattered by elements such as hydrogen (in contrast to X-rays), it makes NR very convenient to detect organic materials in multilayers systems[18]. Herein we propose *i)* to characterize bare duplex nAAO and *ii)* to gain more insights into the PE behavior in nanopores and in particular on the influence of the geometrical constriction present in duplex nAAO on the PE adsorption.

To perform NR on nAAO, a low roughness and strong adhesion of the sample on the substrate, such as Si wafer, is required[19]. As previously observed, Al anodization on Si wafers exhibits different structural characteristics than the anodized aluminum foils and greatly depends on the sputtered Al film morphology tuned by the sputtering conditions[20]. Here duplex nAAO have been synthesized through an anodization/etching/anodization sequence. 0.985 µm thick Al

[a] Sorbonne Université, CNRS, Laboratoire PHENIX, F-75005, Paris, France. Email: nicolas.jouault@sorbonne-universite.fr
[b] Laboratoire Léon Brillouin, CEA Saclay, 91191 Gif-Sur-Yvette, France.

†Electronic Supplementary Information (ESI) available: [Current density curves, SEM analysis, all NR fitting parameters]. See DOI: 10.1039/x0xx00000x

Please do not adjust margins

Please do not adjust margins

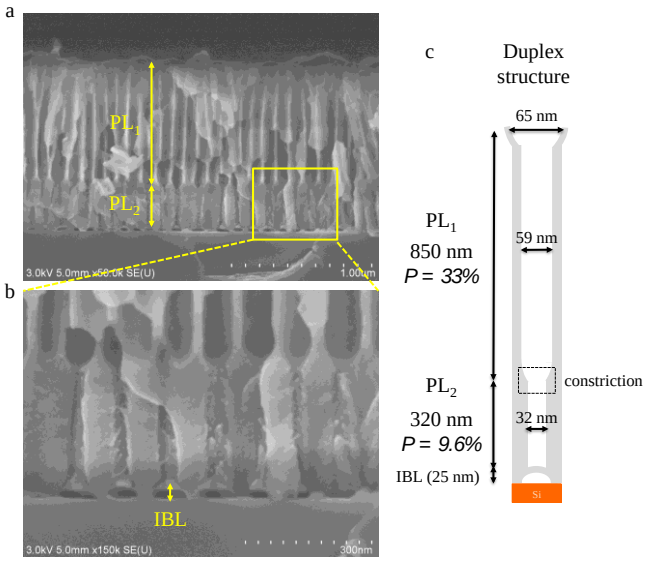


Fig. 1. (a) SEM images of duplex nAAO synthesized on Si wafer. (b) Zoom of the nAAO bottom revealing the inverted barrier layer (IBL). (c) Scheme of the duplex nAAO with the different characteristic sizes.

layer sputtered onto n-type Si wafer (5 mm thick and 2" in diameter) were purchased from ACM (Applications Couches Minces, Versailles, France). A first anodization is carried out in 0.3M oxalic acid under constant voltage (40 V) at a temperature of 18°C during 488 s. Then the nanopores are chemically etched by immersing the wafer in phosphochromic solution (6% wt H_3PO_4 and 1.8% wt CrO_3) during 2h45 at 20°C in order to increase the pore size. Finally the porous nAAO is further anodized under the same previous conditions during 242 s until no Al is left (more synthesis details and current density versus time curves of the two anodizations are given in Fig. S1).

Fig. 1a shows the SEM image of the obtained duplex nAAO. Two connected porous layers (PLs) are clearly observed. The top layer (PL1) is 850 nm thick with a D_p of 59 +/- 4 nm giving a porosity of 33%. The bottom layer (PL2) is 320 nm thick with a D_p of 32 +/- 5 nm giving a porosity of 9.6%. Note that the D_p of both layers have been obtained from analysis of SEM section images. The top surface D_p is 65 +/- 8 nm (slightly larger than the PL1 diameter due to chemical etching during anodization), the pore density is $1.2x10^{10}$ pores/cm^2, the porosity is around 40 % and the interpore distance, D_{int}, is 88 nm (see Fig. S2). D_{int} in the layers are 88+/-9 nm and 94+/-11 nm for PL1 and PL2, respectively. Since the anodizing conditions were the same for the first and second anodizations, similar D_{int} are observed indicating an uniform interface between layers. Fig. 1b shows a zoom of the alumina/Si interface revealing an inverted barrier layer (IBL) of around 25 nm consisting in voids beneath the pores separated by a thin alumina part, as typically observed for anodization on substrate[21, 22]. It might originates from mechanical stress pushing the barrier layer upward and inducing a curvature inversion[23], alumina dissolution due to local temperature increase[21] or oxygen bubbles formation[22].

The bare duplex nAAO is then characterized by NR. NR is a convenient technique to access the thickness and the chemical composition of different layers at the surface of a substrate. The composition is obtained through an important parameter named the scattering length density (SLD) that depends on the interaction between the neutron and the nature of the studied layers and expressed as follows:

$$SLD = \frac{\rho N_a}{M} \sum_i b_i$$

with ρ the density, N_a the Avogadro number, M the molecular weight and b_i the scattering length of atom *i* of the layer. NR is the only technique that can provide accurate experimental SLDs of the different layers without any hypothesis.

During a NR experiment a neutron beam is sent in grazing incidence (i.e. with a low incident angle) on the surface, then is reflected and/or refracted and finally monitored as a function of the scattering vector q. The ratio between the measured intensity and incident intensity in specular condition is called reflectivity, R. The Q dependency of this signal is directly related to the changes in refractive index in the sample along the perpendicular direction to the surface[24]. These changes are characterized by a SLD profile that can be extracted from the fitting of the NR curve. Detailed description of NR principle can be found in reviews 18 and 24. The NR experiments were performed on the HERMES time of flight reflectomer at Laboratoire Léon Brillouin (LLB, CEA Saclay, France) where a neutron pulse (having a large wavelength range from 2 to 22 Å) is sent at a given incident angle. Two angles were used (0.69° and 2°) to access the widest q range and two setup geometries were employed: *i)* measurement in air (SLD_{air} = 0): the neutron beam is sent on the top of the nAAO and *ii)* measurement with a solvent: the neutron beam passes through the silicon wafer which is transparent to neutrons (SLD_{Si} = 2.07 $x10^{-6}$ Å^{-2}). The layer thicknesses above 300 nm cannot be measured due to instrumental resolution but, thanks to the low absorption cross section of alumina, multiple interfaces can be probed deep into the material down to the Si substrate, i.e. PL1/PL2, PL2/IBL and IBL/Si interfaces can be detected. An interface is defined by the gradual SLD changes between layers and the interfacial roughness is the thickness of this interface[18].

Usually the NR is plotted in Rq^4 representation to highlight any features from the layer by compensating the q^{-4} asymptotic decay of the Fresnel reflectivity of Si/Air interface. Fig. 2a shows the Rq^4 representation of the duplex nAAO measured in air with the fit. The NR fitting consists in describing the nAAO as a multilayer system. Each layer is defined by its thickness, SLD and interfacial roughness. The NR fitting is always a delicate process if no structural information is known from another technique, specifically for nAAO. Here we use the SEM images to define a three-layer model: one porous layer with high porosity (PL1), one porous layer with low porosity (PL2) and an IBL supported by Si substrate. Some NR parameters are fixed to the SEM value such as the thicknesses of the two PLs (857 nm and 323 nm respectively).

This journal is © The Royal Society of Chemistry 20xx

Please do not adjust margins

Please do not adjust margins

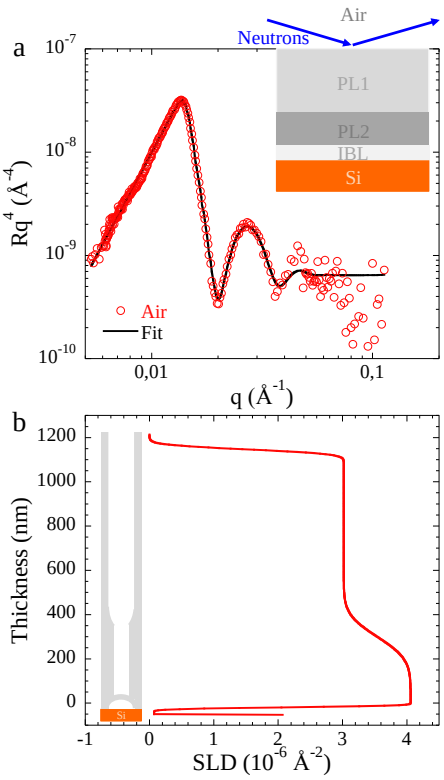


Fig. 2. (a) NR curve in Rq^4 representation for the duplex nAAO measured in air. In insert is shown the R=f(q) representation. The continuous black line corresponds to the best fit based on a three layers model described in the top scheme (χ^2=0.58). (b) SLD profile obtained from the NR fit.

Layer	Thickness (nm)	Roughness (nm)	SLD layer (x10^{-6} Å^{-2})	Porosity (%)	SLD alumina (x10^{-6} Å^{-2})
PL1	850 +/- 11[a]	16.8 +/- 1.6	3.02 +/- 0.02	33.0 +/- 2.4[b]	4.49 +/- 0.02
PL2	320 +/- 15[a]	80 +/- 30	4.06 +/- 0.01	9.6 +/- 1.9[b]	4.49 +/- 0.11
IBL	32.9 +/- 0.1	6.05 +/- 0.05	0.07 +/- 0.03	98.4+/- 0.7[c]	-

Table 1. Results from the fitting of the NR of duplex nAAO in air. [a] These values were fixed during the NR fitting to the ones obtained in SEM. The Si substrate SLD was fixed to 2.07x10^{-6} Å^{-2}. [b] from SEM. [c] Calculated using the IBL SLD.

The IBL thickness, the SLDs and the interfacial roughnesses of the three layers are fitting parameters. The data fitting was performed using the optical matrix method with the *Motofit* program[25] in which the instrumental resolution is also taken into account and the best fit was determined by minimization of the least- squares χ^2 and subsequent visual validation. Table 1 presents the different parameters of the model. The best fit (χ^2 = 0.58) gives a SLD of PL1, PL2 and IBL of 3.02 x10^{-6} Å^{-2}, 4.06 x10^{-6} Å^{-2} and 0.07x10^{-6} Å^{-2}, respectively. Note that the fit is mostly sensitive to the IBL layer and PL2 SLD. Fig. 2b shows the corresponding SLD profile from which the difference in porosities along the nAAO is evidenced. The geometrical constriction, characteristic of the duplex nAAO, is also probed with an extent of 160 +/- 60 nm (twice the PL2 roughness) with a large error bar due to the non-sensitivity of the fit to this parameter. Most interestingly, from the layers SLDs and the porosity known from SEM, the SLD of alumina can be determined with good accuracy: 4.49+/-0.02 and 4.49+/-0.11 x10^{-6} Å^{-2} for PL1 and PL2 respectively. Such direct determination is only possible with NR and provides information about the nAAO layer chemical compositions. Pure amorphous Al_2O_3 with a density of 3.4 g.cm^{-3} has an expected SLD of 4.89 x10^{-6} Å^{-2}, slightly larger than our values. It is well known that nAAO are hydrated and contain some anion impurities coming from the electrolyte used during the anodization (here oxalates), modifying the density, the chemical compositions and thus the SLD. Finally, the thickness of the IBL is 32.9 nm with a roughness of 6.0 nm, in good agreement with the SEM estimation and has a SLD close to air (SLD_{IBL} = 0.07 x10^{-6} Å^{-2}) indicating that this layer is highly porous.

Since several SLD profile might fit the same NR data, NR measurements using several neutron contrasts were performed using different H_2O/D_2O mixtures: 100% D_2O (SLD=6.39x10^{-6} Å^{-2}), 38% D_2O (SLD=2.07x10^{-6} Å^{-2}) and 100% H_2O (SLD=-0.56 x10^{-6} Å^{-2}) to confirm the SLD profile obtained in air. The NR curves are directly simulated using the parameters in air and compared to the experimental data. Assuming that the alumina chemical composition remains unchanged, the layer SLDs were fixed and calculated using the $SLD_{alumina}$ determined in air and the layer porosity *P* as:

$$SLD_{layer} = P * SLD_{solvent} + (1 - P) * SLD_{alumina}$$

The other parameters of the model (thicknesses and interfacial roughness) were all fixed to the values obtained in air (see Table 1). Fig. 3 presents the NR curves with the corresponding simulations. Without any fitting adjustments the NR data can be nicely reproduced with a low χ^2=15.72, 4.03 and 15.16 for 100% D_2O, 38% D_2O and 100% H_2O respectively, confirming unambiguously the profile obtained in air. Moreover, since the nAAO might transform in contact with water[26], a post-H_2O NR measurement was then performed in 100% D_2O. The SLD profile is similar to the first measurement in D_2O (χ^2=2.22, the Rq^4 curves are shown in Fig. S3), indicating that no chemical transformation occurred within the timescale of the different NR measurements, validating our previous hypothesis of no measurable transformation in water. We thus clearly demonstrate that NR is a powerful technique to investigate the structure and composition of duplex nAAO.

To further evidence the NR efficiency on these systems, we propose to study by NR the behavior of polyelectrolytes (PE) in duplex nAAO. Sodium polystyrene sulfonate (NaPSS 70 kDa purchased from Sigma Aldrich) solution was prepared in D_2O (C_0=206.4 g/L (≈ 11% v/v), i.e. within the semi-dilute entangled regime with a correlation length ξ determined by Small-Angle Neutron Scattering of 3.5 nm, a Debye length κ^{-1} of 0.3 nm, and a SLD of 5.77x10^{-6} Å^{-2}) and deposited on top of the duplex nAAO and sealed in a hermetic cell preventing solvent evaporation. NR measurement was performed 30 min after PE deposition.

Fig. 4a shows the Rq^4 NR of the duplex nAAO filled with the NaPSS solution compared to the bare duplex nAAO.

Please do not adjust margins

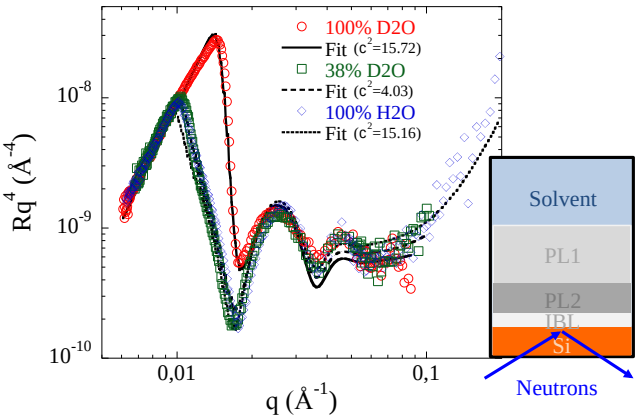


Fig.3. NR curve in Rq^4 representation for the duplex nAAO measured in different H_2O/D_2O mixtures (100% D_2O, 38% D_2O and 100% H_2O). The black lines correspond to the modelling results using a three layers model. All parameters were fixed to the values obtained in air.

Since the PE entering will affect the composition of the layers and might adsorb on top of the pores, the only fitting parameters were the layer SLDs of PL1 and PL2 and the roughness of the PL1/solution interface. The others parameters were fixed. The best fit (χ^2=1.97) is shown in Fig. 4a and Table 2 presents the results. First, the top interfacial roughness increases from 16.8 to 24.7 nm. This difference is around 8 nm, which is close to the radius of gyration (Rg) of the PE, and can be due to possible plugging or PE adsorption[15]. Then, the obtained layers SLDs are lower than the expected theoretical ones if we assume that the PE partitioning K = C_{in}/C_0, (C_{in} being the concentration in the pores) is 1[27] (in that case χ^2=2.78), suggesting that the PE volume fraction inside the pores is higher than in the bulk solution (Fig. 4b). Knowing the nAAO porosities *P*, one can calculate the SLD of the solution inside the pores, SLD_{in}:

$$SLD_{in} = \frac{SLD_{layer} - (1-P)SLD_{alumina}}{P}$$

With these SLD values, a partitioning K of 3.44 and 3.48 is found for PL1 and PL2 respectively. Since the nAAO are positively charged in pure water (pH = 6)[28] and NaPSS is negatively charged, attractive interaction occurs. The SLD_{layer} decrease compared to the theoretical one can be interpreted by the presence of an adsorbed layer inside the pores. The PE adsorbs on the surface, increasing the PE concentration inside the pore compared to the outside bulk solution. In the following, we propose to use the SLD_{layer} extracted from the fit to estimate the surface excess Γ of this adsorbed layer. The SLD_{in} can be decomposed into two contributions as depicted in Fig. 4b: one from the adsorbed PE and one from a PE solution taken at C_0 (i.e. assuming K =1) as:

$$SLD_{in} = f_{ads}SLD_{PSS} + (1-f_{ads})SLD_{PEsolution}$$

with ϕ_{ads} the volume fraction of adsorbed chains in the pores and $SLD_{PE\ solution}$ the SLD of the non adsorbed solution (= 5.77×10^{-6} Å^{-2}). Note that the PE volume fraction inside the

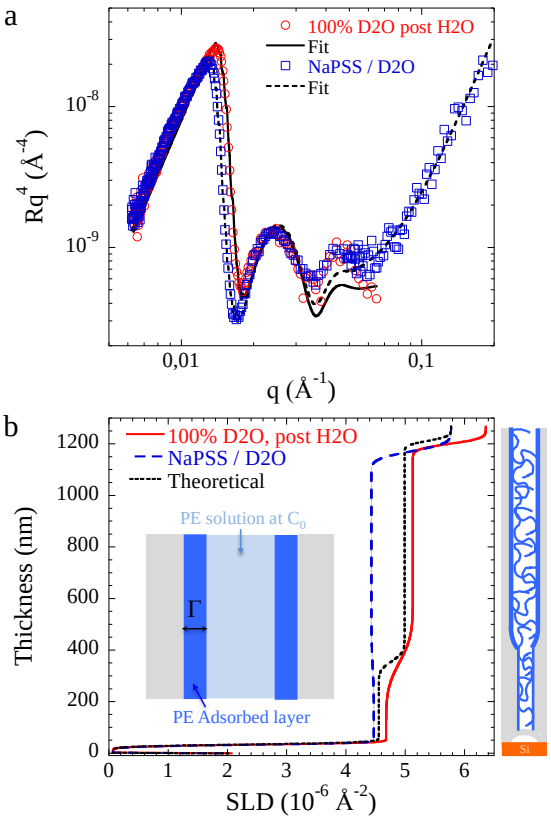


Fig. 4. (a) NR curve in Rq^4 representation for the duplex nAAO measured in 100% D_2O without NaPSS (red circles) and with NaPSS (blue squares). The black lines correspond to the best fits. (b) SLD profile obtained from the NR fit. The theoretical SLD corresponds to the profile obtained if we assume K = 1. Insert: schemes of the PE adsorption model.

Layer	SLD layer ($\times10^{-6}$ Å^{-2})	Roughness (nm)	SLD_{in} ($\times10^{-6}$ Å^{-2})	ϕ_{ads} in pore	Γ (nm)
PL1	4.43+/-0.01	24.7+/-0.8	4.27	0.52	9.0
PL2	4.47+/-0.02	80*	4.25	0.53	5.0

Table 2. Results from the NR fitting of duplex nAAO filled with NaPSS solution. * This value was fixed during the NR fitting.

pores is similar for PL1 and PL2 suggesting that the geometrical constriction doesn't prevent the PE penetration and adsorption, consistent with theoretical work on concentrated neutral polymer penetration where the polymer entering is controlled by the characteristic size ξ [27], which is here smaller than D_p. From ϕ_{ads}, the surface excess Γ of the adsorbed layer can be then calculated as:

$$G = R_p\left[1-(1-f_{ads})^{1/2}\right]$$

with R_p the pore radius. One finds Γ of 9.0 nm and 5.0 nm for PL1 and PL2 respectively. The surface excess is smaller in PL2 suggesting that the pore reduction might control the amount of adsorbed PE but a more systematic study, which is beyond the scope of this paper, is necessary to investigate the exact role of the constriction in this observation.

This journal is © The Royal Society of Chemistry 20xx

Please do not adjust margins

Please do not adjust margins

Conclusions

In this paper we demonstrate that NR is a powerful technique to successfully investigate the structure of duplex nAAO and its composition since it allows direct SLD determination. NR can also detect any changes in SLD profile due to the incorporation of nano-objects into duplex nAAO. To illustrate it we investigate the PE behavior in duplex nAAO and interpreted our NR results by the PE adsorption in the nanopores and the adsorbed layer surface excess can be estimated from NR SLDs. Finally this work shows that NR can be used, through SLDs determination, to quantify PE entering and adsorption and can be further extended to lower C_0 and to different geometrical constriction (smaller in size, ordered or disordered interfaces between layers[10]…).

Conflicts of interest

There are no conflicts to declare.

Acknowledgements

The authors thank LLB for beam time allocation and Didier Lairez for his help during the NR experiments. David Montero is also thanked for his help during SEM sessions. Semfeg instrumentation was provided by the Institut des Matériaux de Paris Centre (IMPC FR2482) and was funded by UPMC, CNRS and by the C'Nano projects of the Région Ile-de-France.

References

1. K. Xiao, L. Wen and L. Jiang, *Small*, 2016, **12**, 2810-2831.
2. C. T. Sousa, D. C. Leitao, M. P. Proenca, J. Ventura, A. M. Pereira and J. P. Araujo, *Applied Physics Reviews*, 2014, **1**, 031102.
3. V. Romero, M. I. Vázquez, S. Cañete, V. Vega, J. García, V. M. Prida, B. Hernando and J. Benavente, *The Journal of Physical Chemistry C*, 2013, **117**, 25513-25518.
4. H. Masuda and K. Fukuda, *Science*, 1995, **268**, 1466-1468.
5. W. Lee and S. J. Park, *Chemical Reviews*, 2014, **114**, 7487-7556.
6. W. Lee, J.-C. Kim and U. Gösele, *Advanced Functional Materials*, 2010, **20**, 21-27.
7. D. Losic and M. Lillo, *Small*, 2009, **5**, 1392-1397.
8. R. Krishnan and C. V. Thompson, *Advanced materials*, 2007, **19**, 988-992.
9. F. Casanova, C. E. Chiang, C.-P. Li and I. K. Schuller, *Applied Physics Letters*, 2007, **91**, 243103.
10. L. Bruschi, G. Mistura, P. Phadungbut, D. D. Do, D. Nicholson, Y. Mayamei and W. Lee, *Langmuir*, 2015, **31**, 4895-4905.
11. G. Mistura, L. Bruschi and W. Lee, *Journal of Low Temperature Physics*, 2016, **185**, 138-160.
12. C. V. Cerclier, M. Ndao, R. Busselez, R. Lefort, E. Grelet, P. Huber, A. V. Kityk, L. Noirez, A. Schonhals and D. Morineau, *Journal of Physical Chemistry C*, 2012, **116**, 18990-18998.
13. R. Lefort, J.-L. Duvail, T. Corre, Y. Zhao and D. Morineau, *The European Physical Journal E*, 2011, **34**, 1-7.
14. L. L. Li, D. S. Zhou, D. H. Huang and G. Xue, *Macromolecules*, 2014, **47**, 297-303.
15. T. D. Lazzara, K. H. A. Lau, A. I. Abou-Kandil, A.-M. Caminade, J.-P. Majoral and W. Knoll, *ACS Nano*, 2010, **4**, 3909-3920.
16. M. Ali, B. Yameen, J. Cervera, P. Ramírez, R. Neumann, W. Ensinger, W. Knoll and O. Azzaroni, *J. Am. Chem. Soc*, 2010, **132**, 8338-8348.
17. L. Javidpour, M. R. R. Tabar and M. Sahimi, *The Journal of Chemical Physics*, 2009, **130**, 085105.
18. F. Cousin and A. Menelle, *EPJ Web of Conferences*, 2015, **104**, 01005.
19. N. P. Hu, X. C. Dong, X. Y. He, S. Argekar, Y. Zhang, J. F. Browning and D. W. Schaefer, *Journal of Applied Crystallography*, 2013, **46**, 1386-1396.
20. A. F. Feil, M. V. da Costa, L. Amaral, S. R. Teixeira, P. Migowski, J. Dupont, G. Machado and S. B. Peripolli, *Journal of Applied Physics*, 2010, **107**, 026103.
21. D. Crouse, Y.-H. Lo, A. Miller and M. Crouse, *Applied Physics Letters*, 2000, **76**, 49-51.
22. S. Z. Chu, K. Wada, S. Inoue and S. Todoroki, *Journal of the electrochemical Society*, 2002, **149**, B321-B327.
23. H.-S. Seo, Y.-G. Jung, S.-W. Jee, J. M. Yang and J.-H. Lee, *Scripta Materialia*, 2007, **57**, 968-971.
24. J. Penfold and R. Thomas, *Journal of Physics: Condensed Matter*, 1990, **2**, 1369.
25. A. Nelson, *Journal of Applied Crystallography*, 2006, **39**, 273-276.
26. X. Carrier, E. Marceau, J.-F. Lambert and M. Che, *Journal of Colloid and Interface Science*, 2007, **308**, 429-437.
27. S. Daoudi and F. Brochard, *Macromolecules*, 1978, **11**, 751-758.
28. B. J. Pedimonte, T. Moest, T. Luxbacher, C. von Wilmowsky, T. Fey, K. A. Schlegel and P. Greil, *Acta biomaterialia*, 2014, **10**, 968-974.

Please do not adjust margins